Food and Chemical Toxicology 126 (2019) 295–302

Contents lists available at ScienceDirect

Food and Chemical Toxicology

journal homepage: www.elsevier.com/locate/foodchemtox

Hypoglycemic activity and gut microbiota regulation of a novel polysaccharide from *Grifola frondosa* in type 2 diabetic mice

Yuqing Chen[a,1], Dan Liu[a,1], Dingyi Wang[b,1], Shanshan Lai[a], Ruting Zhong[a], Yuanyuan Liu[a], Chengfeng Yang[c], Bin Liu[a], Moklesur Rahman Sarker[d], Chao Zhao[a,e,*]

[a] College of Food Science, Fujian Agriculture and Forestry University, Fuzhou, 350002, China
[b] MOE Laboratory of Biosystems Homeostasis & Protection, College of Life Sciences, Zhejiang University, Hangzhou, Zhejiang, 310058, China
[c] College of Food Science and Nutritional Engineering, China Agricultural University, Beijing, 100083, China
[d] Department of Pharmacy, State University of Bangladesh, Dhaka, 1205, Bangladesh
[e] Institute of Chinese Medical Sciences, State Key Laboratory of Quality Research in Chinese Medicine, University of Macau, Macau

ARTICLE INFO

Keywords:
Grifola frondosa polysaccharide
Purification
Hypoglycemic
Intestinal microflora
Single-molecule real-time sequencing

ABSTRACT

GFP-N, a novel heteropolysaccharide with a molecular weight of 1.26×10^7 Da, was isolated from maitake mushroom and purified by anion-exchange chromatography on a DEAE cellulose-52 column and gel-filtration chromatography on a Sephadex G-100 column. Its structure was characterized by Fourier transform infrared spectroscopy and one-dimensional (^{1}H- and ^{13}C-) NMR spectra, ^{1}H−^{1}H correlation spectroscopy, and ^{1}H−^{13}C heteronuclear single-quantum coherence spectroscopy. The structure of GFP-N consisted of L-arabinose, D-mannose and D-glucose and mainly contained three kinds of linkage type units as →2,6)-*α*-D-Man*p*-(1 → 4, *α*-L-Ara*f*-C1→, and →3,6)-*β*-D-Glc*p*-(1 → . GFP-N could activate insulin receptor substrate 1, phosphatidylinositol-3-kinase, and glucose transporter 4 and inhibit c-Jun N-terminal kinase 1/2 for hypoglycemic effects in diabetic mouse livers. This is also the first report of the regulatory efficacy of *Grifola frondosa* polysaccharide on intestinal microflora *in vivo* using single-molecule real-time sequencing. These results indicated that polysaccharide from maitake mushroom could be as an enhancer to improve type 2 diabetes and a healthy food option to help regulate gut microbiota in diabetic individuals.

1. Introduction

Plants have higher efficiency against the diseases and are regarded as a natural treatment source with low-toxicity and various bioactivities (Stefanucci et al., 2018; Zhao et al., 2018b). Type 2 diabetes mellitus (T2DM) is an increasing global health problem. In recent years, considerable attention has been paid to the beneficial effects of phytochemicals on this disease. Plant extracts have great efficacy in producing numerous bioactive molecules dealing with the problem of diabetes mellitus and its associated syndromes (Picot et al., 2017; Mollica et al., 2017a, 2017b). Polysaccharides are a class of important compounds that prevent diabetes mellitus. In addition, they have been demonstrated to possess various physiological and biological activities, such as anti-aging (Chen et al., 2018) and anti-cancerous (Zhang et al., 2017).

Several mushroom species have been used in traditional medicine and have been shown to exert anti-diabetic effects. *Grifola frondosa*, also known as maitake, is a basidiomycete fungus belonging to the Polyporaceae family (Ma et al., 2015). Various functional constituents of *G. frondosa* have drawn considerable attention worldwide. *G. frondosa* contains an average dry weight of 33.53% and 47.84% carbohydrates in fruiting bodies and mycelia, respectively (Huang et al., 2011), and a high amount of (1 → 3,1 → 6)-*β*-D-glucans account for 13.2% of the water-soluble polysaccharides (Su et al., 2016). Cui et al. (2013) found that *G. frondosa* polysaccharide (GFP) was composed of (1 → 3)-linked-*β*-D-Man*p*, (1 → 3,6)-linked-*β*-D-Man*p*, and (1 → 6)-linked-*α*-D-Gal*p*. GFP represents an important active substance with various biological functions, such as immunomodulatory (Cui et al., 2006; Meng et al., 2017), antidiabetic (Chen et al., 2018), anti-nephritic (Kou et al., 2019), antioxidative (Chen et al., 2012), antitumoral (Fan et al., 2011), antimicrobial (Gu et al., 2006), and antiviral (Zhao et al., 2016) activities.

Statistics from the International Diabetes Federation (IDF) revealed that 8.3% of adults have diabetes among 382 million people worldwide.

* Corresponding author. No.15 Shangxiadian Rd., Cangshan District, Fuzhou, 350002, China.
E-mail address: zhchao@live.cn (C. Zhao).
[1] Yuqing Chen, Dan Liu and Dingyi Wang contributed equally to this work.

https://doi.org/10.1016/j.fct.2019.02.034
Received 6 December 2018; Received in revised form 20 February 2019; Accepted 23 February 2019
Available online 28 February 2019
0278-6915/

As a prevalent chronic disease, T2DM is characterized by insulin resistance (IR) and abnormal glucose metabolism. The insulin pathway is a crucial target in preventing and controlling diabetes. Regulating glucose by increasing insulin sensitivity or insulin secretion helps regulate glucose metabolism in insulin-resistant target tissues (Tian et al., 2016). Phosphatidylinositol-3-kinase (PI3K), insulin receptor substrate 1 (IRS1), and glucose transporter 4 (GLUT4) play crucial roles in glucose metabolism and insulin resistance. The mechanism begins with the stimulation of insulin receptor intrinsic kinase activity to activate PI3K signaling. Then, PI3K inhibits the c-Jun N-terminal kinase 1 (JNK1) activity in succession. Moreover, GLUT4, which is regulated by insulin, is able to reduce glucose levels through participating in the IRS/PI3K signaling pathway (Chen et al., 2018). Since most antidiabetic drugs for diabetes have significant side effects, effective and low-toxicity drugs are urgently needed.

It has been verified that the alteration of gut microbiota is a new vital factor in the development of insulin resistance and T2DM (Zhao et al., 2018c). Gut microbiota may be related to disruptions in host metabolism, such as IR (Turnbaugh et al., 2006). Currently, multiple kinds of carbohydrates have various effects on intestinal ecology via gut symbionts (Shang et al., 2017). Polysaccharides could potentially improve gut health and play a dominant role in forming and changing the bacterial community composition of the human gut (Fu et al., 2018; Zhao et al., 2018c). However, the effect of GFP on the gut microbiota changes is unclear in recent research. Single-molecule real-time (SMRT) sequencing technology enables the depiction of the entire gut microbiota profile by a noncultivation-based approach. Several studies have shown that SMRT is powerful in depicting the 16S rRNA gene-based profile of microbiota present in a wide range of samples. Compared with second-generation sequencing, it can read, on average, 5,000–15,000 bp, a few hundred base-pairs longer than before with more sensitivity and accuracy (Lee et al., 2016).

The impacts of oral GFP administration on host hyperglycemia and gut microbes have not yet been reported. In our previous research, the antidiabetic potential of *G. frondosa* polysaccharide was determined only in IR-HepG2 cells (Chen et al., 2018). The antidiabetic potential of the purified water-extractable heteropolysaccharides isolated from *G. frondosa* and their molecular mechanisms are insufficient at present. Therefore, we identified the structural characteristics and properties of a novel GFP-N and its antidiabetic activity in streptozotocin-induced type 2 diabetic mice. Furthermore, this is the first report of the regulatory efficacy of *G. frondosa* polysaccharides on the gene expression profile and intestinal microflora *in vivo* by SMRT.

2. Materials and methods

2.1. Preparation of G. frondosa polysaccharide

The dried powders (50 g) prepared from *G. frondosa* were extracted with hot ultrapure water (1:30, g/mL) by an ultrasonic extractor at 50 kHz for 30 min. After further extraction in a water bath at 90 °C for 3 h, the suspension was centrifuged at 5000 rpm for 15 min and concentrated with a vacuum evaporator at 65 °C. Four volumes of anhydrous ethanol were added to concentrated GFP. The crude GFP was removed protein by the Sevag method and dialyzed by 7 kDa Mw cutoff dialysis membranes for 48 h. The samples were fractionated with a column (2.6 cm × 60 cm) of DEAE cellulose-52 (Beijing Solarbio Science & Technology Co., Ltd, China) and column (1.6 cm × 100 cm) of Sephadex G-100 (Beijing Solarbio Science & Technology Co., Ltd, China) with 0.1 mol/L NaCl. The collected liquid was monitored with the phenol-sulfuric acid (Li et al., 2009). The main purified fraction named GFP-N was collected after dialysis for 48 h and lyophilized for further studies.

2.2. Molecular weight analysis of GFP-N

The molecular weight of GFP-N was determined by a MALLS system (Wyatt Technology, Santa Babara, USA), which was coupled with gel permeation chromatography (GPC) (Agilent, USA) and a refractive index detector for analysis. The chromatographic system was composed of a degasser, a high-performance pump, an injection valve fitted with a 1 mL loop and a GPC column (Shodex OHpak SB-806 HQ, Showa Denko, Tokyo, Japan), which were connected in tandem. The GFP-N (10 mg/mL) dissolved in 0.1 mol/L NaCl was filtered before injection and eluted with the degassed and 0.1 mol/L NaCl in ultrapure water at a flow rate of 0.5 mL/min. The dn/dc value of GFP-N was 0.135 mL/g at 658 nm and 25 °C. The data were recorded and analyzed with Astra V software.

2.3. Gas chromatography (GC) analysis

The monosaccharide composition was measured by our previous methods (Chen et al., 2018; Zhao et al., 2016). Dried GFP-N (10 mg) was dissolved in 2 mL of trifluoroacetic acid (2 mol/L) and hydrolyzed for 6 h at 100 °C. The soluble fraction was dried with running nitrogen. The product mixed with hydrochloric acid hydroxyl (10 mg) and Ac_2O-pyridine (0.5 mL) and incubated at 90 °C for 30 min and further incubated with 0.5 mL of acetic anhydride at 90 °C for 30 min. A GC equipped with an HP-5MS capillary column (0.25 mm × 30 m × 0.25 μm) and a flame ionization detector was used to determine the monosaccharide concentration. All products were carried by gaseous nitrogen. Conditions were as follows: an injector temperature of 250 °C, a detector temperature of 250 °C, and a column temperature of 210 °C.

2.4. Fourier transform infrared (FT-IR) spectroscopy

The mixture (10 mg dried GFP-N with 200 mg KBr) was pressed into 1.0 mm thick or less for infrared analysis. FT-IR spectra were recorded on a Perkin-Elmer spectrum GX FT-IR system (PerkinElmer, USA) in the region of 4000–400 cm^{-1}. The major peaks (intensity and wavenumber) of GFP-N were identified and analyzed using the instrument software (EZ OMNIC 6.0, Thermo Electron Corporation, Madison, USA).

2.5. Nuclear magnetic resonance (NMR) spectroscopy analysis

Structural characterization of GFP-N was analyzed by one- and two-dimensional NMR investigations. Twenty milligrams of GFP-N were dissolved in CD_3OD and lyophilized three times. ^1H and ^{13}C-NMR spectra of GFP-N were recorded on a 600-MHz Bruker INNOVA 600 NB NMR spectrometer and a 500 MHz Bruker NMR spectrometer (Bruker, Rheinstetten, Germany) at 25 °C, respectively. Heteronuclear single-quantum correlation (HSQC) and two-dimensional correlated spectroscopy (COSY) were also used for GFP-N identification. Two-dimensional NMR experiments were performed in phase-sensitive mode and carried out following the standard operating procedures of the Bruker Company. The chemical shifts of NMR were calculated by using MestReNova 8.0 software (Mestrelab Research, Escondido, USA).

2.6. Animals, diabetes induction and experimental design

Male ICR mice (18–22 g) provided by Fuzhou General Hospital of Nanjing Military Region (FGHNMR) were housed in sanitized polypropylene cages (SPC) under a well-maintained and hygienic environment (temperature 22 ± 2 °C, 55 ± 5% humidity, and 12 h/12 h light/dark cycle) and had free access to basic chow and water. All experimental protocols were approved by the board of FGHNMR (No. FZJQ2011018). After one week, 10 mice were randomly selected as the normal group and continued to feed on basic chow, and all the others were used for type 2 diabetic animal models by the previous method

(Zhao et al., 2018a). These mice were then regrouped as follows: control group and GFP-N treatment groups that were treated with 75 and 150 mg/kg body weight. Animals in the normal and control groups were given saline daily.

2.7. Assessment of hypoglycemic activity

The FBG and body weight were measured after GFP-N treatment for 0, 14, and 28 days. FBG levels were detected by OMRON Active Glucose Monitor (Kyoto, Japan). After gavage with GFP-N for 4 weeks, all mice were fasted for 12 h with free access to water for the oral glucose tolerance test, which is usually used to test for diabetes, insulin resistance, and rarer disorders of carbohydrate metabolism. Animals were orally administrated with 2 g/kg glucose. Blood glucose was measured at 0, 0.5, and 2 h after glucose administration. The area under curve (AUC) value was used for estimating the ability to regulate blood sugar and calculated as follows: $AUC = 0.5\ (G_{0\ h} + G_{0.5\,h}) \times 0.5 + 0.5\ (G_{2\ h} + G_{0.5\,h}) \times 1.5$.

2.8. Analysis of glycated hemoglobin and β-cell function

The blood of mice was collected, and the clear serum was separated for the measurement of glycated hemoglobin (HbA1c) and fasting serum insulin (FSI) by ELISA Kits (Mlbio, China). Homeostatic model assessment (HOMA) was used to quantify insulin resistance and β-cell function. HOMA-β values were measured based on the values of FBG and FSI, which were calculated as follows: $HMOA\text{-}\beta = (20 \times FSI)/(FBG\text{-}3.5)$.

2.9. Histopathological analysis

All animals were anatomized after an intraperitoneal injection of 7% chloral hydrate (0.5 mL/100 g body weight). The liver and kidney were fixed in 10% formalin after excision and washing. The paraffin-embedded 2-mm tissue slices were stained by hematoxylin and eosin (H &E) for histopathological analysis.

2.10. Bioinformatic analysis of gut microbiota in response to GFP-N by SMRT

The DNA of the excrement of each animal was extracted using an OMEGA DNA isolation kit (Omega, D5625-01, USA) according to the manufacturer's instructions. The specific 16-bp barcode sequence was added to the primer in the conserved region. PCRs contained 5 μL of Q5 reaction buffer (5 ×), 5 μL of Q5 High-Fidelity GC Buffer (5 ×), 0.25 μL of Q5 High-Fidelity DNA Polymerase (5 U/μL), 2 μL (2.5 mM) of dNTP mixture, 2 μL (10 μM) of primers 27F (5′-AGAGTTTGATCMTGG CTCAG-3′) and 1492R (5′-ACCTTGTTACGACTT-3′), 2.5 ng of DNA template, and up to 25 μL of ddH_2O. The following thermal cycling conditions were used: initial denaturation at 98 °C for 2 min; followed by 25/10 cycles consisting of denaturation at 98 °C for 30 s, annealing at 55 °C for 30 s, and extension at 72 °C for 90 s; and a final extension at 72 °C for 5 min. PCR amplification products were purified by Agencourt AMPure Beads (Beckman Coulter, Indianapolis, IN), quantified using the PicoGreen dsDNA Assay Kit (Invitrogen, Carlsbad, CA, USA) and then sequenced using the PacBio Sequel System. Raw data were processed by applying the PacBio SMRT Link portal (version 5.0.1.9585). The restrictive filtering parameters of minimum full passes, minimum predicted accuracy, and maximum read length of inserts were set at 3, 99, and 2000, respectively. The bioinformatic analysis was performed on the extracted high-quality sequences using the Quantitative Insights Into Microbial Ecology (QIIME) package (Version 1.8.0, http://qiime.org). The high-quality unique sequences were classed into operational taxonomic units (OTUs) at the threshold of 97% similarity by UCLUST. The significance of differentiation of microbiota structure among groups was assessed by PERMANOVA (permutational multivariate analysis of variance) and ANOSIM (analysis of similarities) using R package "vegan". The taxonomy compositions and abundances were visualized using MEGAN and GraPhlAn.

2.11. RNA extraction and real-time PCR

Total RNA from liver tissues was extracted using an RNA extraction kit (Takara, Japan). The PrimeScript™ RT reagent Kit (Takara, Japan) was used for cDNA synthesis. Real-time PCR of JNK1/2, IRS1, PI3K, GLUT4, and glyceraldehyde-3-phosphate dehydrogenase (GAPDH) was conducted to monitor gene expression levels using SYBR Green PCR Master Mix (Takara, Japan) on an AB7300 Real-Time PCR system (Applied Biosystems, Foster City, USA). The specific primers listed were as follows: JNK1, F: 5′-CAGAAGCAAACGTGACAAC-3′, R: 5′-AAGAAT GGCATCATAAGCTG-3'; JNK2, F: 5′-CAAGGGATTGTTTGTGCTGC-3′, R: 5′-TGGTTCTGAAAAGGACGGCT-3'; IRS1, F: 5′-AAGGAGGTCTGGCAG GTTATC-3′, R: 5′-ATGGTCTTGCTGGTCAGGC-3'; PI3K, F: 5′-CCAAAT GAAAAGAACGGCTA-3′, R: 5′-GCGACTTCAGCTTATCATGG-3'; GLUT4, F: 5′-AACGGATAGGGAGCAGAAACCCAA-3′, R: 5′-GTGCAAAGGGTGA GTGAGGCATTT-3′, and GAPDH, F: 5′-TGAAGCAGGCATCTGAGGG-3′, R: 5′-CGAAGGTGGAAGAGTGGGAG-3'. The reaction conditions were as follows: initial activation at 95 °C for 30 s, followed by 45 cycles of denaturation at 95 °C for 3 min, annealing at 57 °C for 7 s, and extension at 72 °C for 15 s. The relative expression levels of target mRNAs were normalized by GAPDH signals.

2.12. Western blot analysis

The total protein of liver tissues was extracted by RIPA lysis, and its concentration was determined using a BCA protein assay kit (Pierce, Rockford, IL). Proteins were subjected to SDS-PAGE and transferred to immunoblot PVDF membranes (Millipore, Billerica, MA). The PVDF membranes were blocked with blocking buffer for 2 h at 37 °C. The membranes were incubated at 4 °C overnight with the primary antibody solutions, including GAPDH, IRS1, JNK1/2, PI3K, or GLUT4 (Abcam, Cambridge, UK), and further incubated with anti-rabbit antibodies conjugated to alkaline phosphatase for 1 h at 37 °C. The membranes were washed four times with TBS-Tween 20 (TBST) after each incubation. Immunolabeled proteins were visualized by the BCIP/NBT Alkaline Phosphatase Color Development Kit (Beyotime, Shanghai, China).

2.13. Statistical analysis

The dates of all experiments are expressed as the mean ± SD. Statistical analyses were performed using SPSS (ANVOA, SPSS 16.0), and $p < 0.05$ was considered significant.

3. Results and discussion

3.1. Purification, monosaccharide composition, and molecular weight analysis of GFP-N

GFP-N was separated and purified successively using DEAE cellulose-52 and Sephadex G-100 column chromatography with 0.1 mol/L NaCl solutions as the mobile phase (Fig. 1). One peak in the logarithmic plot of the molecular weight of GFP-N appeared at 9.46–16.27 min (Fig. 1a). The average molecular weight (*Mw*) of GFP-N was 1.26×10^7 Da, and the molar masses (*Mn*) was 6.90×10^6 Da. The analysis of monosaccharides of GFP-N by GC was observed (Supplementary Fig. S1). It mainly consisted of L-arabinose, D-mannose and D-glucose with molar ratios of 3.79:1.00:49.70.

3.2. FT-IR spectra analysis of GFP-N

FT-IR spectra recorded in the region 4000–400 cm^{-1} were used to

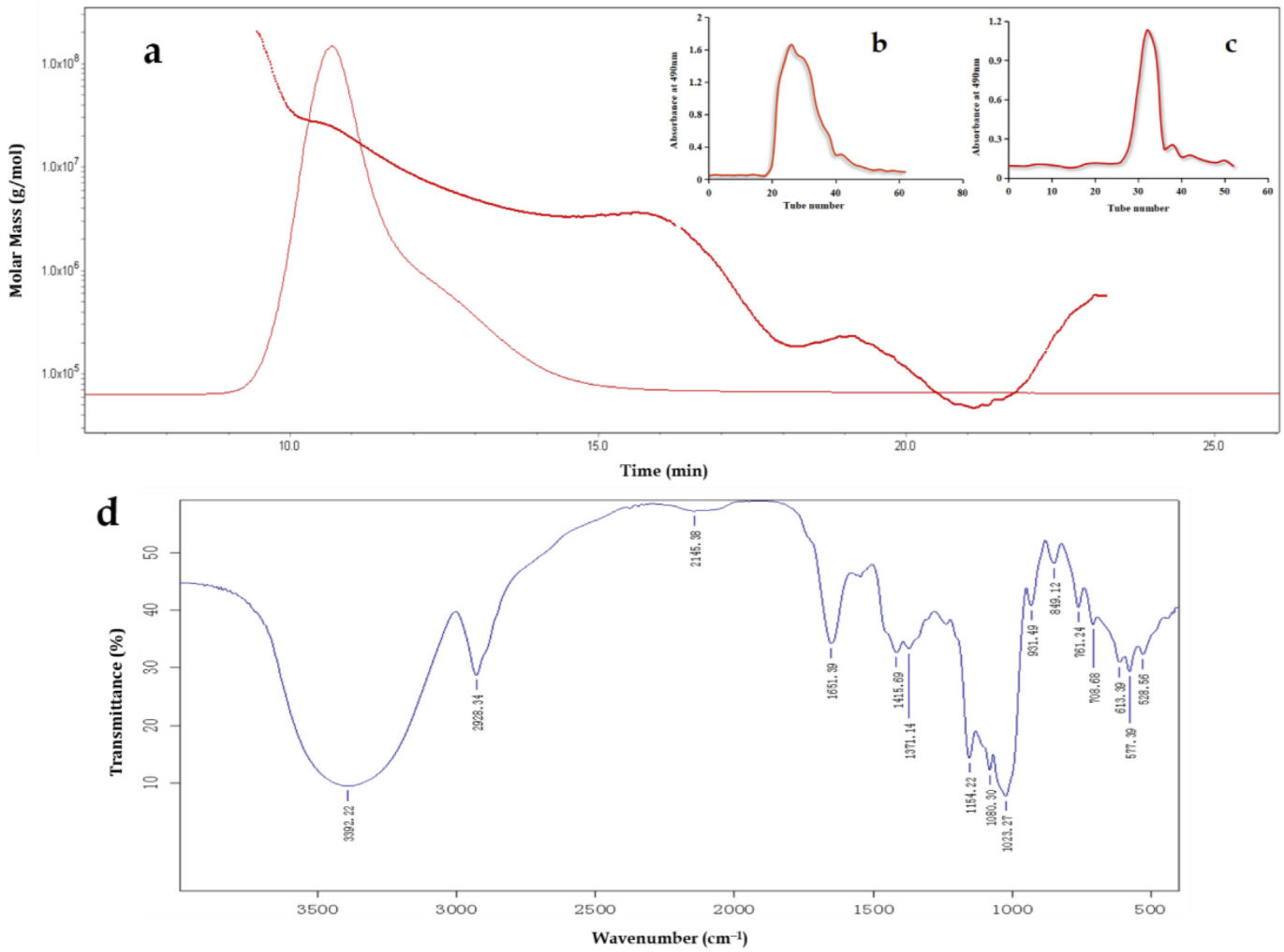

Fig. 1. Logarithmic plots of molecular weight (a) of GFP-N in GPC/MALLS system and its purification by DEAE cellulose-52 (b) and Sephadex G-100 (c) column chromatography. And FT-IR analysis (d) of GFP-N at 4000 to 400 cm^{-1} in the carbohydrate region.

detect the structure of GFP-N (Fig. 1d). In the spectrum, a strong O—H stretching vibration of the sugar ring was observed at 3392 cm^{-1}. The absorption peak of 2928 cm^{-1} was the C—H stretching vibration band of methyl or methylene. The peaks from 1400 to 1200 cm^{-1} represented C—H bending vibration. These regions have displayed the structural features of polysaccharides. In addition, the two stretching vibration peaks at 1154 cm^{-1} and 1080 cm^{-1} in the spectrum suggested the presence of C—O—C and C—O—H (Zhao et al., 2016). Disappearance of the peaks at 1750 cm^{-1} manifested the absence of carboxyl functional groups (Chen et al., 2015). Moreover, the absorption peaks in the 1419–1030 cm^{-1} region suggested the presence of pyranoside (Ma et al., 2015; Yu et al., 2009). The absorption peak at 1080 cm^{-1} also showed that GFP-N contained the β-glucosidic linkages of the glucosyl residues. The weak absorption peak at 931 cm^{-1} was characteristic of pyranose, while the peak at 761 cm^{-1} corresponded to the stretching vibration of D-pyranose.

3.3. NMR analysis

The results of GFP-N by ^{1}H and ^{13}C-NMR spectra are given in Fig. 2. The chemical shifts in the ranges of 0.9–2.0 and 3.2–5.5 ppm in the ^{1}H-NMR spectrum display the characteristics of carbohydrates (Zhao et al., 2016). No absorption peak was found at approximately 6.5–9.5 ppm, which showed the existence of aromatic characteristics. The absorption peaks at 4.1–2.5 ppm indicated the transformation of hydrogen atoms from H-2 to H-6 in glycosidic bonds (Cheng and Neiss, 2012; Zhao et al., 2016). Three major different anomeric carbon signals (98.54, 99.89, and 102.37 ppm) were detected at 90–110 ppm in ^{13}C-NMR (Fig. 2b). No chemical shifts appeared at approximately 82–88 ppm, which suggested the pyranose ring of GFP-N, consistent with the results mentioned above (Fan et al., 2006). The resonances of C-2 to C-5 on the glycosidic ring at 65–79 ppm were observed. The C-6 for pyranoside was found at 60.57 ppm. The structural characterization of GFP-N was also detected for structure by GFP-N by ^{1}H—^{1}H COSY and ^{1}H—^{13}C HSQC (Supplementary Fig. S2; Supplementary Table S1). The signals were analyzed and found that GFP-N consisted mainly of three kinds of sugar residues: →2,6)-α-D-Man*p*-(1 → 4, α-L-Ara*f*-C1→ and →3,6)-β-D-Glc*p*-(1→ (Bilan et al., 2010; Li et al., 2006; Wang et al., 2014). According to these studies, there was no reported structural component the same as GFP-N. It could be concluded that GFP-N was a novel polysaccharide isolated from *G. frondosa*.

3.4. Effect of GFP-N on body weight in diabetic mice

The variation in the body weight of mice was measured on days 0, 14, and 28 of treatment (Supplementary Fig. S3). Few alterations were observed in the normal groups, but the body weight of the control group decreased compared with that on day 0 of treatment. The body weight of the GFP-N group after treatment was obviously lower than that of the control group ($p < 0.01$). Furthermore, high-dose GFP-N

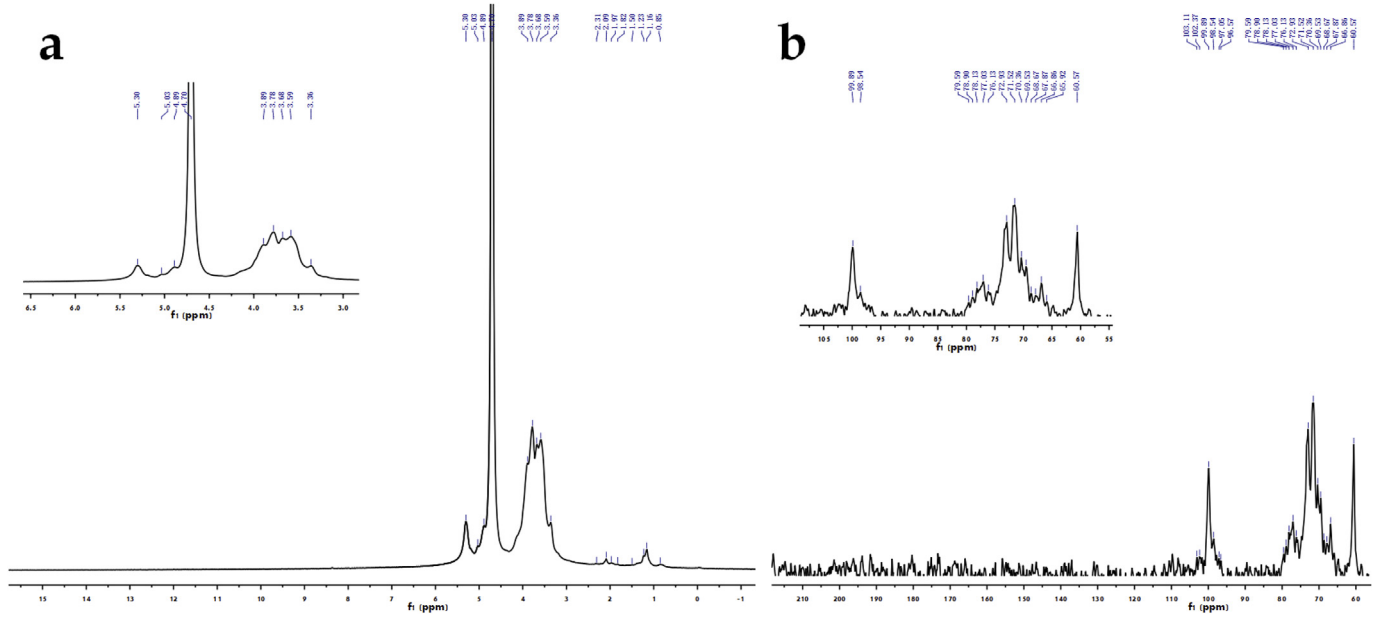

Fig. 2. ^{1}H- (a) and ^{13}C- (b) NMR spectral analysis of GFP-N recorded in CD_3OD.

treatment could increase the weight of mice in the short time period and effectively improve diabetic symptoms.

3.5. Effect of GFP on blood parameters

The effect of GFP-N on FBG levels in diabetic mice after treatment is shown in Fig. 3A. After 28 days of treatment, the FBG level of the mice was significantly lower than that of the control group ($p < 0.05$). Mice treated with low-dose GFP-N (M-75) showed decreased FBG levels compared with high-dose GFP-N (M-150) on the 14th day. As an indicator, glucose tolerance plays a crucial role in reflecting the degree of T2DM. The AUC of glucose in different groups is shown in Fig. 3B. The integrated AUC for glucose was significantly higher in the control group than that in the normal group ($p < 0.05$), which indicated that diabetic

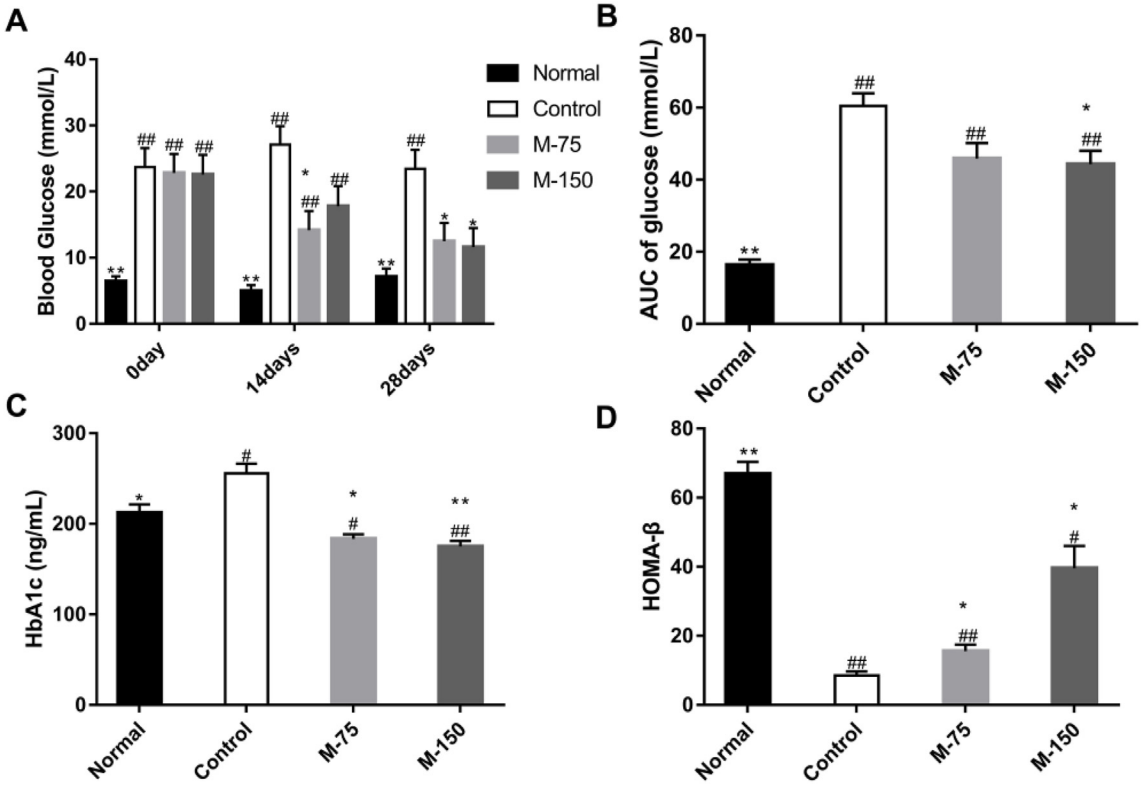

Fig. 3. The effects of blood glucose levels (a), and oral glucose tolerance (b), HbA1c (c), and HOMA-β (d) in streptozotocin/high fat diet-induced type 2 diabetic mice after treatment with GFP-N at 75 mg/kg body weight (M-75) and 150 mg/kg body weight (M-150). Values are expressed as mean ± SD (n = 8). $^{*}p < 0.05$, $^{**}p < 0.01$ indicated statistical significance compared with control group, respectively; while $^{\#}p < 0.05$, $^{\#\#}p < 0.01$ indicated statistical significance compared with normal group.

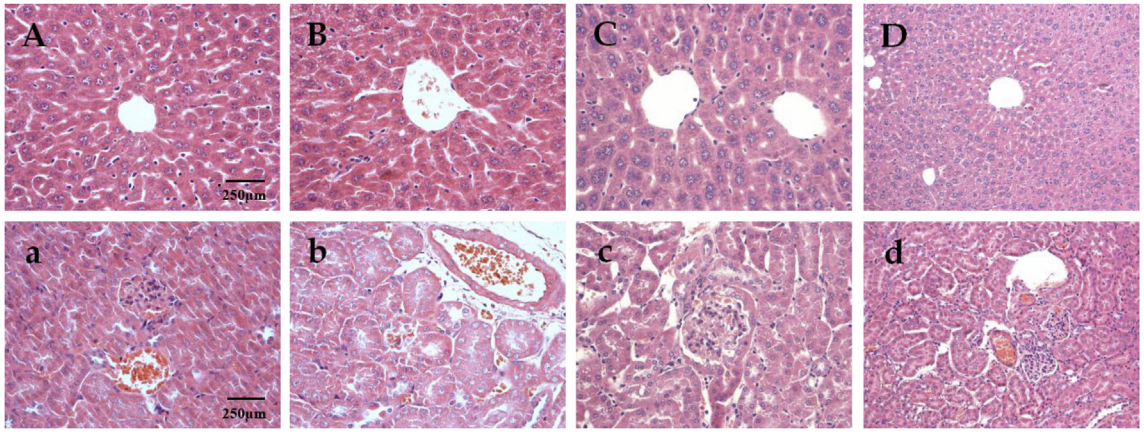

Fig. 4. Effects of GFP-N on histomorphological changes of the liver (A–D) and kidney (a–d) in mice (Hematoxylin and eosin staining, 400 ×). A & a: normal group; B & b: control group; C & c: low-dose GFP-N (M-75) group; D & d: high-dose GFP-N (M-150) group.

mice showed significant impairment in glucose tolerance to exogenously administered glucose. GFP-N treatment showed a significantly lower AUC value than that of diabetic animals, particularly at a dose of 150 mg/kg body weight. Four weeks after treatment, GFP-N significantly decreased the HbA1c values ($p < 0.05$) (Fig. 3C). Meanwhile, GFP-N enhanced the HOMA-β level and improved the function of islet β-cells in diabetic mice (Fig. 3D). These results indicated that mice fed with GFP-N could maintain normal biochemical blood parameter levels.

3.6. Effect of GFP-N on the histopathology of the liver and kidney

Histological analysis of H&E-stained liver and kidney sections was conducted (Fig. 4). The hepatocytes of mice in the normal group were arranged in an orderly manner and distributed radially around hepatic cords (Fig. 4A). The dispersive hepatocyte and collapse of the hepatic lobule in the control group indicated local hepatocyte necrosis and moderate portal inflammation (Fig. 4B). By comparison, the liver inflammation symptoms were significantly ameliorated through GFP-N treatment. Moreover, GFP-N at 150 mg/kg showed a relatively orderly arrangement of the choroid structure and efficient amelioration of lipid accumulation in hepatocytes (Fig. 4D). The renal tubule was tightly sealed with the renal corpuscle, and the nephrocytes were arranged regularly in the normal group (Fig. 4a). However, an increased in the volume and number of glomerulus cells and the glomerulus edema phenomenon of epithelial cells occurred in the control group (Fig. 4b). However, GFP-N administration relieved the inflammation developed in the kidney and weakened the vacuolation of renal epithelial cells. The volume of the renal corpuscle decreased in both the low- and high-dose GFP-N groups, and the nephrocytes were more neatly arrayed, especially in the high-dose group (Fig. 4c and d).

3.7. Effects of GFP-N on the insulin signaling pathways

Real-time qPCR and western blotting were carried out to analyze the mRNA and protein expression of key genes in the insulin signaling pathway (Fig. 5). The transcription of IRS1 and PI3K was limited in the control group when compared with the normal group. The mRNA expression of JNK1/2 increased significantly and indicated that abnormal gene transcription of the insulin signaling pathway eventually led to decreased transshipment capacity of glucose and insulin resistance. GFP-N at both dose levels upregulated the mRNA expression of IRS1 and PI3K and downregulated the expression of JNK1/2 mRNA significantly (Fig. 5A). The same results were achieved in the protein expression (Fig. 5B). In the low-dose GFP-N treatment group, the PI3K level was increased and JNK1 was reduced significantly (Supplementary Fig. S4). IRS1 plays an important role as a mediator of insulin and cytokine signaling conduction. When insulin is combined with the insulin receptor located in the membrane of myocytes, the insulin receptor autophosphorylates and catalyzes the tyrosine phosphorylation of IRS1, which then binds to PI3K and subsequently activates molecular Akt/PKB. These steps ultimately are activated, resulting in the translocation of GLUT4 from an intracellular pool to the plasma membrane of myocytes to reinforce glucose transport. GLUT4 participates in the IRS/PI3K insulin signaling pathway through Akt, which inhibits the activity of JNK, which indirectly affects the adequate regulation of insulin by IRS1/PI3K (Chen et al., 2018). The results mentioned above demonstrated that GFP-N can improve glucose consumption and alleviate the condition of insulin resistance by increasing the expression of IRS1/PI3K/GLUT4 genes/proteins and decreasing the expression of JNK1/2 genes/proteins, thus improving glucose uptake in the liver.

3.8. Species abundance and structure analysis of gut microflora

According to the OTU classification and determination, the bacterial phyla of gut microbiota were classified using R language (Fig. 6a). Compared with diabetic control mice, the number of Bacteroidetes significantly increased, but the content of Firmicutes and Proteobacteria decreased in the fecal samples of the GFP-N-fed mice. The decrease in Bacteroidetes bacteria and the increase in bacterial abundance of Firmicutes were related to the increase in dietary energy absorption and low level of inflammation (Turnbaugh et al., 2006). The ratio of Bacteroidetes and Firmicutes was positively correlated with the blood glucose concentration (Larsen et al., 2010). Verrucomicrobiae may be a potential marker of T2DM as it had a significantly lower abundance in both the pre-DM and T2DM groups. At the species level, the composition of gut microbiota in the GFP-N-treated group was generally similar to that in the normal group but exhibited large differences when compared with the control group (Fig. 6b). After GFP-N treatment, the relative abundances of *Porphyromonas gingivalis*, *Akkermansia muciniphila*, *Lactobacillus acidophilus*, *Tannerella forsythia*, *Bacteroides acidifaciens*, and *Roseburia intestinalis* were increased significantly. Glycemic levels in diabetes are affected by the persistence of *P. gingivalis* (Makiura et al., 2008). *A. muciniphila* was the first intestinal microbial isolate of the phylum Verrucomicrobia and was more abundant in T2DM patients compared to healthy controls (Qin et al., 2012). The probiotic bacteria *L. acidophilus* exhibited a significant delaying effect on the progression of diabetes induced by high fructose administration in rats (Yadav et al., 2007). *B. acidifaciens* has potential for the treatment of metabolic diseases, such as diabetes and obesity (Yang et al., 2017). The microbiome of type 2 diabetic patients is

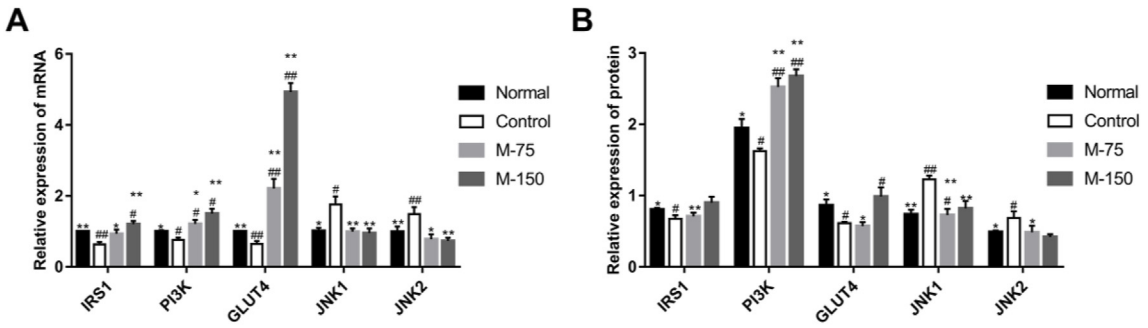

Fig. 5. Effects of GFP-N on gene expression of liver tissue in mice. (a) Effects of GFP-W treatment on the mRNA expression levels of IRS1/PI3K/JNK and GLUT4; (b) Signals were normalized with those of GAPDH and western blot analysis. $^{*}p < 0.05$, $^{**}p < 0.01$ indicated statistical significance compared with control group, respectively; while, $^{\#}p < 0.05$, $^{\#\#}p < 0.01$ indicated statistical significance compared with normal group.

characterized by the depletion of several butyrate-producing bacteria, including *Roseburia intestinalis*. Interestingly, the GFP-N intake induced the interaction between the intestinal microbiome and host antidiabetic effects, such as the genera *Alloprevotella*, *Alistipes*, *Barnesiella*, *Blautia*, *Desulfovibrio*, and *Parabacteroides*. An increased relative abundance of putative SCFA-producing bacteria, including *Alloprevotella* and *Blautia*, promotes the remission of inflammation, insulin resistance, and T2DM by reducing the intestinal endotoxins released into the circulation (Zhang et al., 2018). Among the bacteria, *Alistipes* was positively correlated with inflammation and hyperglycemia but negatively correlated with pancreas weight (Zhao et al., 2018a; Zheng et al., 2018). The elevated abundance of *Alistipes* is closely associated with diabetes development (Patterson et al., 2016). The genus *Barnesiella* might have anti-inflammatory protection in mice. However, bacteria that increased in the gut of type 2 diabetic patients also include *Parabacteroides* and the sulphate-reducing bacteria *Desulfovibrio* (Stefanaki et al., 2017). GFP-N significantly maintained the homeostasis of gut microbiota.

4. Conclusion

A novel polysaccharide from the *G. frondosa* fruiting body named GFP-N was isolated and purified. It mainly consists of three kinds of sugar residues →2,6)-α-D-Man*p*-(1 → 4, α-L-Ara*f*-C1→ and →3,6)-β-D-Glc*p*-(1 → . GFP-N treatment decreased the fasting blood glucose level, improved oral glucose tolerance, alleviated insulin resistance, and protected against liver and kidney injury with reduced inflammation in diabetic mice. In particular, it ameliorated hepatic insulin resistance by regulating the IRS1/PI3K and JNK signaling pathways. Moreover, the higher Bacteroidetes abundance and lower Firmicutes and Proteobacteria abundances were significantly present in the GFP-N-treated groups. GFP-N also regulated the bacterial structure by increasing the species abundance of *Akkermansia*, *Lactobacillus*, and *Turicibacter*. Hence, the polysaccharide from *G. frondosa* has the potential to be a natural source of functional foods and auxiliary hypoglycemic drugs.

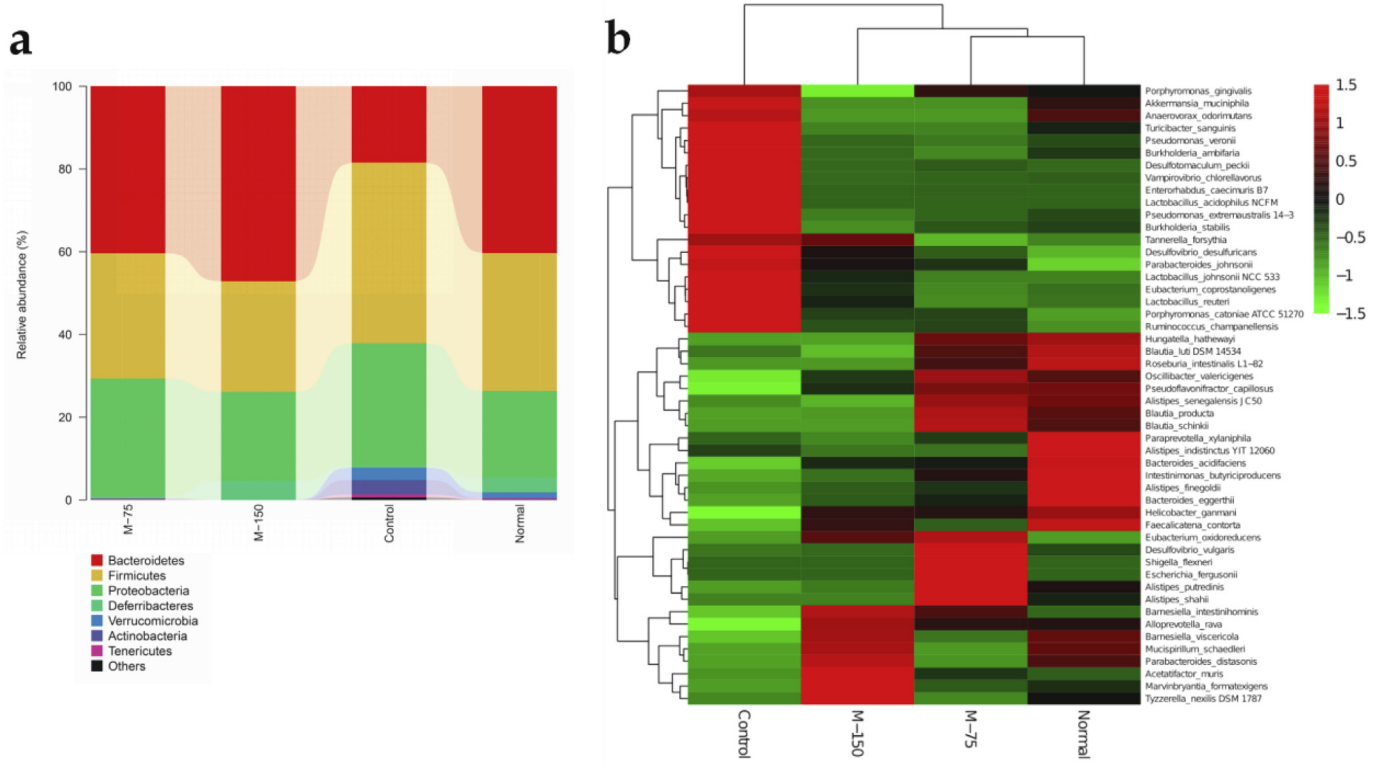

Fig. 6. Effects of GFP-N on relative abundance of gut microbiota at the phylum (a) and species (b) levels.

Declaration of interest

The authors declare that there is no conflict of interest that could be perceived as prejudicing the impartiality of the research reported.

Acknowledgements

This work was financially supported by Project of Fuzhou Municipal Bureau of Science and Technology (2017-N-36 & 2018-G-87) and National Natural Science Foundation of China (81741163). The project was also supported International Science and Technology Cooperation Programme (KXb16011A) of Fujian Agriculture and Forestry University.

Appendix A. Supplementary data

Supplementary data to this article can be found online at https://doi.org/10.1016/j.fct.2019.02.034.

Transparency document

Transparency document related to this article can be found online at https://doi.org/10.1016/j.fct.2019.02.034.

References

Bilan, M.I., Grachev, A.A., Shashkov, A.S., Kelly, M., Sanderson, C.J., Nifantiev, N.E., Usov, A.I., 2010. Further studies on the composition and structure of a fucoidan preparation from the brown alga *Saccharina latissima*. Carbohydr. Res. 345 (14), 2038–2047.

Chen, G.T., Ma, X.M., Liu, S.T., Liao, Y.L., Zhao, G.Q., 2012. Isolation, purification and antioxidant activities of polysaccharides from *Grifola frondosa*. Carbohydr. Polym. 89 (1), 61–66.

Chen, L., Liu, J., Zhang, Y., Dai, B., An, Y., Yu, L., 2015. Structural, thermal, and anti-inflammatory properties of a novel pectic polysaccharide from Alfalfa (*Medicago sativa* L.) stem. J. Agric. Food Chem. 63, 3219–3228.

Chen, Y.Q., Liu, Y.Y., Sarker, M.M.R., Yan, X., Yang, C.F., Zhao, L.N., Lv, X.C., Liu, B., Zhao, C., 2018a. Structural characterization and antidiabetic potential of a novel heteropolysaccharide from *Grifola frondosa* via IRS1/PI3K-JNK signaling pathways. Carbohydr. Polym. 198, 452–461.

Chen, Y.X., Liu, X.Y., Wu, L.X., Tong, A.J., Zhao, L.N., Liu, B., Zhao, C., 2018b. Physicochemical characterization of polysaccharides from *Chlorella pyrenoidosa* and its anti-ageing effects in *Drosophila melanogaster*. Carbohydr. Polym. 185, 120–126.

Cheng, H.N., Neiss, T.G., 2012. Solution NMR spectroscopy of food polysaccharides. Polym. Rev. 52 (2), 81–114.

Cui, F.J., Tao, W.Y., Xu, Z.H., Guo, W.J., Xu, H.Y., Ao, Z.H., Jin, J., Wei, Y.Q., 2006. Structural analysis of anti-tumor heteropolysaccharide GFPS1b from the cultured mycelia of *Grifola frondosa* GF9801. Bioresour. Technol. 98 (2), 395–401.

Cui, F.J., Zan, X.Y., Li, Y.H., Yang, Y., Sun, W.J., Zhou, Q., Yu, S.L., Dong, Y., 2013. Purification and partial characterization of a novel anti-tumor glycoprotein from cultured mycelia of *Grifola frondosa*. Int. J. Biol. Macromol. 62, 684–690.

Fan, J.M., Zhang, J.S., Tang, Q.J., Liu, Y.F., Zhang, A.Q., Pan, Y.J., 2006. Structural elucidation of a neutral fucogalactan from the mycelium of *Coprinus comatus*. Carbohydr. Res. 341 (9), 1130–1134.

Fan, Y.N., Wu, X.Y., Zhang, M., Zhao, T., Zhou, Y., Han, L., Yang, L.Q., 2011. Physical characteristics and antioxidant effect of polysaccharides extracted by boiling water and enzymolysis from *Grifola frondosa*. Int. J. Biol. Macromol. 48 (5), 798–803.

Fu, X., Cao, C.L., Ren, B.B., Zhang, B., Huang, Q., Li, C., 2018. Structural characterization and *in vitro* fermentation of a novel polysaccharide from *Sargassum thunbergii* and its impact on gut microbiota. Carbohydr. Polym. 183, 230–239.

Gu, C.Q., Li, J.W., Chao, F. Hua, 2006. Inhibition of hepatitis B virus by D-fraction from *Grifola frondosa*: synergistic effect of combination with interferon-alpha in HepG2 2.2.15. Antivir. Res. 72 (2), 162–165.

Huang, S.J., Tsai, S.Y., Lin, S.Y., Liang, C.H., Mau, J.L., 2011. Nonvolatile taste components of culinary-medicinal maitake mushroom, *Grifola frondosa* (Dicks.:Fr.) S.F. gray. Int. J. Med. Mushrooms 13, 265–272.

Kou, L., Du, M.Z., Liu, P.J., Zhang, B.H., Zhang, Y.Z., Yang, P., Shang, M.Y., Wang, X.D., 2019. Anti-diabetic and anti-nephritic activities of *Grifola frondosa* mycelium polysaccharides in diet-streptozotocin-induced diabetic rats via modulation on oxidative stress. Appl. Biochem. Biotechnol. 187 (1), 310–322.

Larsen, N., Vogensen, F.K., van den Berg, F.W.J., Nielsen, D.S., Andreasen, A.S., Pedersen, B.K., Al-Soud, W.A., Sorensen, S.J., Hansen, L.H., Jakobsen, M., 2010. Gut microbiota in human adults with type 2 diabetes differs from non-diabetic adults. PLoS One 5 (2) e9085.

Lee, H., Gurtowski, J., Yoo, S., Nattestad, M., Marcus, S., Goodwin, S., McCombie, W.R., Schatz, Michael, 2016. Third-generation sequencing and the future of genomics. bioRxiv. https://doi.org/10.1101/048603.

Li, B., Wei, X.J., Sun, J.L., Xu, S.Y., 2006. Structural investigation of a fucoidan containing a fucose-free core from the brown seaweed, *Hizikia fusiforme*. Carbohydr. Res. 341 (9) 1135–114.

Li, F., Yuan, Q.P., Rashid, F., 2009. Isolation, purification and immunobiological activity of a new water-soluble bee pollen polysaccharide from *Crataegus pinnatifida* bge. Carbohydr. Polym. 78 (1), 80–88.

Ma, X.L., Li, C.J., Qi, W.T., Li, X.R., Wang, S.X., Cao, X.H., Wang, C.L., 2015. Protective effect of extracellular polysaccharides from *Grifola frondosa* mycelium on CCl_4-injured liver *in vitro*. Bioactive Carbohydrates and Dietary Fibre 6, 7–14.

Makiura, N., Ojima, M., Kou, Y., Furuta, N., Okahashi, N., Shizukuishi, S., Amano, A., 2008. Relationship of Porphyromonas gingivalis with glycemic level in patients with type 2 diabetes following periodontal treatment. Oral Microbiol. Immunol. 23 (4), 348–351.

Meng, M., Cheng, D., Han, L., Chen, Y., Wang, C., 2017. Isolation, purification, structural analysis and immunostimulatory activity of water-soluble polysaccharides from *Grifola frondosa* fruiting body. Carbohydr. Polym. 157, 1134–1143.

Mollica, A., Zengin, G., Locatelli, M., Stefanucci, A., Novellino, E., 2017a. An assessment of the nutraceutical potential of *Juglans regia* L. leaf powder in diabetic rats. Food Chem. Toxicol. 107 (Pt B), 554–564.

Mollica, A., Zengin, G., Locatelli, M., Stefanucci, A., Mocan, A., Macedonio, G., Carradori, S., Onaolapo, O., Onaolapo, A., Adegoke, J., Olaniyan, M., Aktumsek, A., Novellino, E., 2017b. Anti-diabetic and anti-hyperlipidemic properties of *Capparis spinosa* L.: *In vivo* and *in vitro* evaluation of its nutraceutical potential. J. Funct. Foods 35, 32–42.

Patterson, E., Ryan, P.M., Cryan, J.F., Dinan, T.G., Ross, R.P., Fitzgerald, G.F., Stanton, C., 2016. Gut microbiota, obesity and diabetes. Postgrad. Med. 92 (1087), 286–300.

Picot, M.C.N., Zengin, G., Mollica, A., Stefanucci, A., Mahomoodally, M.F., 2017. *In vitro* and *in silico* studies of mangiferin from *Aphloia theiformis* on key enzymes linked to diabetes type 2 and associated complications. Med. Chem. 13 (7), 633–640.

Qin, J., Li, Y., Cai, Z., Li, S., Zhu, J., Zhang, F., Liang, S.S., Zhang, W.W., Guan, Y.L., Shen, D.Q., Peng, Y.Q., Zhang, D.Y., Jie, Z.Y., Wu, W.X., Qin, Y.W., Xue, W.B., Li, J.H., Han, L.C., Lu, D.H., Wu, P.X., Dai, Y.L., Sun, X.J., Li, Z.S., Tang, A.F., Zhong, S.L., Li, X.P., Chen, W.N., Xu, R., Wang, M.B., Feng, Q., Gong, M.H., Yu, J., Zhang, Y.Y., Zhang, M.M., Hansen, T., Sanchez, G., Raes, J., Falony, G., Okuda, S., Almeida, M., LeChatelier, F., Renault, P., Pons, N., Batto, J.M., Zhang, Z.X., Chen, H., Yang, R.F., Zheng, W.M., Li, S.G., Yang, H.M., Wang, J., Ehrlich, S.D., Nielson, R., Pedersen, O., Kristiansen, K., Wang, J., 2012. A metagenome-wide association study of gut microbiota in type 2 diabetes. Nature 490, 55–60.

Shang, Q., Jiang, H., Cai, C., Hao, J., Li, G., Yu, G., 2017. Gut microbiota fermentation of marine polysaccharides and its effects on intestinal ecology: an overview. Carbohydr. Polym. 179, 173–185.

Stefanaki, C., Peppa, M., Mastorakos, G., Chrousos, G.P., 2017. Examining the gut bacteriome, virome, and mycobiome in glucose metabolism disorders: are we on the right track? Metabolism 73, 52–66.

Stefanucci, A., Zengin, G., Locatelli, M., Macedonio, G., Wang, C.K., Novellino, E., Mahomoodally, M.F., Mollica, A., 2018. Impact of different geographical locations on varying profile of bioactives and associated functionalities of caper (*Capparis spinosa* L.). Food Chem. Toxicol. 118, 181–189.

Su, C.H., Lai, M.N., Lin, C.C., Ng, L.T., 2016. Comparative characterization of physicochemical properties and bioactivities of polysaccharides from selected medicinal mushrooms. Appl. Microbiol. Biotechnol. 100, 4385–4393.

Tian, Y.M., Liu, Y., Wang, S., Dong, Y., Su, T., Ma, H.J., Zhang, Y., 2016. Anti-diabetes effect of chronic intermittent hypobaric hypoxia through improving liver insulin resistance in diabetic rats. Life Sci. 150, 1–7.

Turnbaugh, P.J., Ley, R.E., Mahowald, M.A., Magrini, V., Mardis, E.R., Gordon, J.I., 2006. An obesity-associated gut microbiome with increased capacity for energy harvest. Nature 444 (7122), 1027–1031.

Wang, Y., Shen, X.K., Liao, W.F., Fang, J.P., Chen, X., Dong, Q., Ding, K., 2014. A heteropolysaccharide, l-fuco-d-manno-1,6-α-d-galactan extracted from *Grifola frondosa* and antiangiogenic activity of its sulfated derivative. Carbohydr. Polym. 101 (1), 631–641.

Yadav, H., Jain, S., Sinha, P.R., 2007. Antidiabetic effect of probiotic dahi containing *Lactobacillus acidophilus* and *Lactobacillus casei* in high fructose fed rats. Nutrition 23 (1), 62–68.

Yang, J.Y., Lee, Y.S., Kim, Y., Lee, S.H., Ryu, S., Fukuda, S., Hase, K., Yang, C.S., Lim, H.S., Kim, H.M., Ahn, S.H., Kwon, B.E., Ko, H.J., Kweon, M.N., 2017. Gut commensal bacteroides acidifaciens prevents obesity and improves insulin sensitivity in mice. Mucosal Immunol. 10 (1), 104–116.

Yu, J., Cui, P.J., Zeng, W.L., Xie, X.L., Liang, W.J., Lin, G.B., Zeng, L., 2009. Protective effect of selenium-polysaccharides from the mycelia of *Coprinus comatus* on alloxan-induced oxidative stress in mice. Food Chem. 117, 42–47.

Zhang, F., Shi, J.J., Thakur, K., Hu, F., Zhang, J.G., Wei, Z.J., 2017. Anti-cancerous potential of polysaccharide fractions extracted from peony seed dreg on various human cancer cell lines via cell cycle arrest and apoptosis. Front. Pharmacol. 8, 102.

Zhang, B.W., Sun, W.L., Yu, N., Sun, J., Yu, X.X., Li, X., Xing, Y., Yan, D., Ding, Q.Z., Xiu, Z.L., Ma, B.P., Yu, L.Y., Dong, Y.S., 2018. Anti-diabetic effect of baicalein is associated with the modulation of gut microbiota in streptozotocin and high-fat-diet induced diabetic rats. J. Funct. Foods. 46, 256–267.

Zhao, C., Gao, L.Y., Wang, C.Y., Liu, B., Jin, Y., Xing, Z., 2016. Structural characterization and antiviral activity of a novel heteropolysaccharide isolated from *Grifola frondosa* against enterovirus 71. Carbohydr. Polym. 144, 382–389.

Zhao, C., Yang, C.F., Chen, M.J., Lv, X.C., Liu, B., Yi, L.Z., Cornara, L., Wei, M.C., Yang, Y.C., Tundis, R., Xiao, J.B., 2018a. Regulatory efficacy of brown seaweed *Lessonia nigrescens* extract on the gene expression profile and intestinal microflora in type 2 diabetic mice. Mol. Nutr. Food Res. 62 (4), 1700730.

Zhao, C., Yang, C.F., Liu, B., Lin, L., Sarker, S.D., Nahar, L., Yu, H., Cao, H., Xiao, J.B., 2018b. Bioactive compounds from marine macroalgae and their hypoglycemic benefits. Trends Food Sci. Technol. 72, 1–12.

Zhao, C., Yang, C.F., Wai, S.T.C., Zhang, Y.B., Portillo, M.Y., Paoli, P., Wu, Y.J., Cheang, W.S., Liu, B., Carpene, C., Xiao, J.B., Cao, H., 2018c. Regulation of glucose metabolism by bioactive phytochemicals for the management of type 2 diabetes mellitus. Crit. Rev. Food Sci. https://doi.org/10.1080/10408398.2018.1501658.

Zheng, J.P., Yuan, X.B., Cheng, G., Jiao, S.M., Feng, C., Zhao, X.M., Yin, H., Du, Y.G., Liu, H.T., 2018. Chitosan oligosaccharides improve the disturbance in glucose metabolism and reverse the dysbiosis of gut microbiota in diabetic mice. Carbohydr. Polym. 190, 77–86.